Comparing the Cycle-to-Cycle Variations of Pulsing Spray Characteristics by Means of Ensemble Image and Probability Presence Image Analysis Techniques

Jie Zhong[1,2], David L.S. Hung[1,2*], Zhenkan Wang[2], Yuyin Zhang[2], Min Xu[2]

[1]University of Michigan-Shanghai Jiao Tong University Joint Institute, Shanghai, China
[2] National Engineering Laboratory for Automotive Electronic Control Technology, Institute of Automotive Engineering, Shanghai Jiao Tong University, Shanghai, China

Abstract

This paper presents an investigation to reveal the cycle-to-cycle variations of pulsing spray characteristics of Spark-Ignition Direct-Injection (SIDI) fuel injectors. The objective is to quantify the spray's cycle-to-cycle variation such that further insight of the operating principles in the fuel injection system could be developed to enhance the combustion efficiency and reduce emissions of SIDI engines. The experiments were carried out using a multi-hole SIDI fuel injector under an extended range of test conditions in a spray chamber. Using a strobe light as an illumination source, images of the spray structure were taken by a CCD camera. The analysis approach of the cycle-to-cycle variation was based on constructing two types of images, namely, 1) Ensemble Image, and 2) Probability Presence Image (PPI). The analysis of the ensemble image and PPI reveals that both approaches can be used to extract the variations of the spray structure. While an ensemble image is useful for determining the quantitative variation of the spray characteristics, such as the penetration and spray angle, in terms of average, maximum and minimum limits, a PPI provides a new way to examine the spray variation in terms of a probability defined for the presence of the liquid region. Not only a PPI is able to illustrate the magnitude of cycle-to-cycle variation in penetration and spray angle values quantitatively, it also displays the variations qualitatively in a two-dimensional manner in terms of the liquid presence probability.

Introduction

Spark-Ignition Direct-Injection (SIDI) engines are designed to inject fuel directly into the combustion chamber and possess the potential benefits of enhanced fuel economy, faster transient response, and lower cold-start hydrocarbon emission, among others [1]. In a SIDI engine, the quality of fuel mixture determines the successful ignition and proper burn rate for high quality engine performance. However, large cycle-to-cycle variations in the fuel mixture may increase the covariance of indicated mean effective pressure [2], thereby leading to combustion instabilities that may result in passenger-perceived engine roughness and transient vehicle vibration [3].

The fuel injector is considered as a critical component in the SIDI fuel system. Generally, most of the requirements of the SIDI injector are similar to that of port fuel injector, such as they both require the small pulse-to-pulse variation in fuel quantity and spray characteristics. In certain areas, the specification criteria of a SIDI injector are more stringent. For example, SIDI injectors focus more on the spray penetration control with smaller flow variance under large thermal gradients. They should also withstand higher temperature at the injector body and tip [1]. Since the mixture formation process in a SIDI engine is very important, the study of spray characteristics is of great significance [4]. In this paper, we emphasize the study of the cycle-to-cycle variation in pulsing spray characteristics of SIDI fuel injectors through the use of optical diagnostic (image-based) analysis techniques.

Optical diagnostic techniques have evolved as a versatile measurement tool in recent years. Programmable hardware and automated data post-processing algorithms have enhanced the efficiency in data reduction and analysis [5]. Different optical techniques, such as stroboscopic technique, light extinction method, laser-induced florescence, phase Doppler interferometry, laser Doppler velocimetry and photographic imaging [6-11] have been developed and applied in a variety of flow measurements relating to engine flow and combustion applications. Among these techniques, photographic imaging is especially useful for qualifying and quantifying the global characteristics of fuel spray over the injection period. By using optical diagnostic techniques, many researchers have investigated the influence of various factors such as fuel properties, fuel injection pressure, back pressure, and fuel temperature that affect the spray characteristics [12-20].

This work extends to a wider range from the previous work of fuel spray cycle-to-cycle characterization [21, 22] to explore various factors which may affect the spray cycle-to-cycle variation at a deeper understanding by using a direct photographic imaging method. The experiments of this study were carried out using a multi-hole

* Corresponding author: dhung@sjtu.edu.cn

SIDI fuel injector in a spray chamber: three types of fuel (n-heptane, ethanol and gasoline), two fuel injection pressures (5 MPa and 10 MPa), three levels of back pressure (50 kPa, 101 kPa and 500 kPa absolute pressure) and three fuel injection-temperatures (-10 °C, 25 °C and 80 °C). Mie-scattered images of the spray structure were taken by a CCD camera using a strobing white light. The analysis approach of this work to reveal the cycle-to-cycle variation is based on image processing and analysis.

Experimental Methods & Analysis Procedure

1) Experimental Apparatus & Test Procedure

The spray behavior is investigated by means of a strobe light illumination to obtain the geometrical characteristics of spray in terms of spray angle and penetration. Figure 1 demonstrates the schematic of the experimental apparatus, (which consists of a constant volume chamber, a fuel supply system, a fuel temperature control system, a chamber pressurization system, a vacuum system and a photographic imaging system). An eight-hole injector (the outside hole diameter was estimated to be about 0.2 mm) was installed vertically at the top of the constant volume chamber. Four quartz windows surrounding the chamber provided full optical access, and back pressure in the chamber from 20kPa (absolute) to 2MPa was regulated by a nitrogen supply and a vacuum pump. A piston accumulator with a separate nitrogen supply system was used to provide the required fuel pressure. In addition, a specially-fabricated injector with a thermocouple embedded near its tip was used to correlate the fuel temperature inside the injector with the temperature of water running through a coolant path surrounding the injector. Therefore, the fuel temperature in the injector could be regulated by controlling the temperature of the running water near the injector.

Spray images were captured by the LaVision imaging system which consisted of a CCD camera which located at an angle of 150° from the light source. A timing device to control the image acquisition timing and the injection event was synchronized by the Davis® software. The experimental matrix was selected to represent various operating conditions of the injection system as shown in Table 1, where the ambient temperature was fixed at 25°C. The test fuels, namely, n-heptane, ethanol and gasoline were chosen because they exhibited different physical properties, as shown in Table 2. The injection pressure, the back pressure in the chamber and the fuel temperature were varied to investigate their influence on the spray cycle-to-cycle variation.

Table 1 Experimental conditions.

Test fuels	N-heptane, Ethanol, Gasoline
Ambient temperature (℃)	25
Ambient absolute pressure (kPa)	50,101,500
Fuel temperature (℃)	-10,25,80
Injection pressure (MPa)	5(only n-heptane),10

Table 2 Physical properties of the test fuels.

25°C	N-heptane	Ethanol	Gasoline
Liquid Viscosity (mPa·s,)	0.38	1.05	0.38
Liquid Density (kg/m^3)	679	783	750
Surface tension (mN/m)	19.8	22.5	22.1

The spray characteristics illustrated in Fig. 2 are defined according to the SAE J2715 recommended practice on gasoline fuel injection spray measurements and reporting [23]. The spray penetration is defined as the lowest vertical distance to the injector tip. The spray angle is defined as the widest angle including all plumes in the image. For each test condition of Table 1, a series of spray images as well as background images were recorded. The background image was subtracted from the spray image during image processing. Fifty images were taken at 1.3 ms after the start of fuel (ASOF). The images were processed using the Matlab® image processing toolbox.

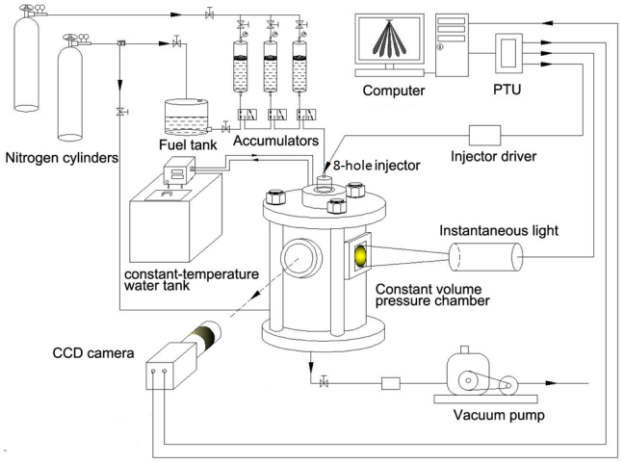

Figure 1 Schematic Layout of Experimental Apparatus

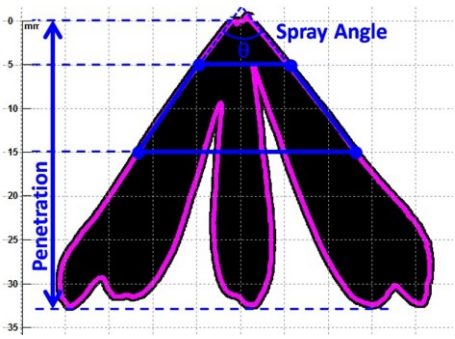

Figure 2 Definitions of Spray Characteristics.

2) Image Analysis Procedure and Methodology

The development of the image processing technique to reveal the cycle-to-cycle variation of pulsing spray is a major objective of this work. The strobe light image of every single fuel injection provides detailed spatial and

temporal information into a peculiar spray event. The analysis approach includes constructing two types of images, i.e., 1) Ensemble Image, and 2) Probability Presence Image (PPI).

The Ensemble Image is obtained by averaging the intensity value of each image from a series of test replicates at the same time delay after the injection logic pulse. This conventional image processing method is used to extract the overall characteristics of fuel spray, such as spray penetration and spray angle on a statistically valid basis. The intensity (grayscale value) of the Ensemble Image indicates the average information of the liquid presence.

The Probability Presence Image (PPI) is constructed by the following steps. First, the region of the liquid fuel presence in each image is identified by a thresholding method and binarized images are obtained. According to the 'Image Processing Handbook' by John C. Russ [24], the 'the simplest method' of threshing methods is used in our analysis by locating the peaks in the histogram of images and setting the thresholds midway between them. By observing the histograms, the peaks are located in 12 and 37 on the full 256 levels (8 bit). Using this thresholding method, the threshold is set to 25 (about 10% of the 8 bit greyscale) so that any pixel with grey level lower than 25 are set to 0, and those with grey levels above the threshold are set to 1. Then, the binarized values of all images are added pixel-by-pixel in the same test replicates (i.e., the same ASOF images taken from the injection repetitions), and then the value is divided by the total number of images. Third, the value of these images at each pixel location is multiplied by the maximum luminance intensity of the image format (for our work, the maximum luminance value of an 8-bit image is 255), and then the ensemble PPI was formed as a grayscale image. For an 8-bit image, the pixels with a grayscale value of 255 on the PPI imply the 100% probability of liquid presence, while those with value of 0 represent no liquid presence and 0% probability.

It is worth mentioning that the PPI, formed by using a set of binarized images, is also an ensemble image but illustrated with the probability of liquid presence. It provides another approach to examine the cycle-to-cycle variation. The numerical value of the probability represents the core region where the liquid is always present over the cycles considered. For instance, the outermost periphery indicates where the liquid may be least likely to exist beyond this boundary, which is of a low probability value. However, since the original liquid image is binarized, there is no account for the different cycles of liquid presence. It is simply a measure of whether liquid is present at the designated SOI time delay.

In accords with constructing two types of images, the data analysis procedure applies these two indexes, namely, 1) the coefficient of variation (COV), and 2) the Probability Variation Index (PVI), to indicate the variation of each method. The coefficient of variation (COV) of the spray characteristics obtained from repetitive images that are formed as the Ensemble Image is a useful dimensionless number to indicate the dispersion from the average response and can be used to make comparison between data sets of different units. The standard equations to calculate the variations of the spray characteristics are shown below:

$$\mathrm{average}(x) = \sum_{i=1}^{n} x_i / n \tag{1}$$

$$\mathrm{SD}(x) = \sqrt{\sum_{i=1}^{n} (x_i - \mathrm{average}(x))^2 / (n-1)} \tag{2}$$

$$\mathrm{COV}(x) = \mathrm{SD}(x) / \mathrm{average}(x) * 100\% \tag{3}$$

where x represents any one of the spray characteristics defined above and n means the number of images. For the PPI, a Probability Variation Index (PVI) is defined to demonstrate how much variation exists from the 5% liquid presence probability. The equation is shown below:

$$\mathrm{PVI} = (x(5\%) - x(95\%)) / x(5\%) \tag{4}$$

where x(5%) represents the value of any one of the spray characteristics at the 5% spray liquid presence probability and x(95%) is defined in the same way. From the above equations, the COV is an indication of variation relative to the mean value, while PVI implies the variation range based on the least probability.

3) Checks for Variation due to Hardware Configurations

Before the tests were performed, it was realized that the hardware systems including the camera, strobe light, injection driver and etc. could produce variation which could be considered erroneously as part of the spray cycle-to-cycle variation. To address some of these intrinsic variations, several tests were designed to check for variation due to hardware configurations. For example, consecutive pulses of injector driving current and the injection pulse signal were collected and measured. Figure 3 depicts the ten overlapped consecutive injection pulses and their current response of the injector. No distinct difference in the injector response behavior was observed. The opening and closing time delays of the current responses were very consistent, with their coefficients of variation being less than 0.19% and 0.02%, respectively. The fluctuations in injection pressure, back pressure, fuel temperature and ambient temperature were monitored in the experiments. The variations of fuel temperature and ambient temperature were held within ±0.1°C, and the variations of back pressure and fuel in-

jection pressure were ±1 kPa and ±10 kPa, respectively. In addition, to validate the stable performance of the imaging system and strobe light, 50 images of a printed spray photo were taken successively. As depicted in Fig. 4 using the PPI approach, the ratio of 1% over 100% PPI area was 1.02 being close to unity. The fifty images are almost overlapped with very limited variation. Therefore, it is believed that the imaging system could perform properly with high repeatability, and the hardware did not play a major role in the images of spray cycle-to-cycle variation.

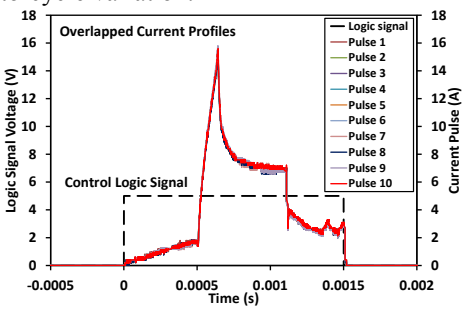

Figure 3 Overlapped injector responses to ten consecutive control signal pulses

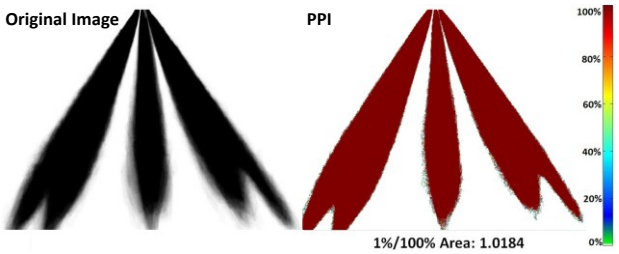

Figure 4 The PPI result of fifty images taken over the same printed spray photo

Results and Discussion

Results are elaborated in four subsections to discuss the effect of fuel type, injection pressure, back pressure and fuel temperature on the spray cycle-to-cycle variation to achieve a deeper understanding of the spray characteristics by comparing the information extracted from the ensemble image and PPI.

1) Effects of Fuel Types

The ensemble images and PPIs of the spray of three different fuels were obtained and analysed as shown in Figure 5. The spray images were taken at the condition of 10 MPa injection pressure, 100 kPa back pressure with the fuel temperature and ambient temperature being 25 °C. The scale on the left side of images shows the length of the spray from the injector tip while the color bar on the right side of the PPIs indicates different percentages of the liquid presence probability. The ensemble images show a typical nature of the spray shape with smooth edges of the plumes since the ensemble average blends the variations in the original images. The PPIs illustrates of the variation distribution of the overall spray liquid presence. The variation grows more along with the spray penetration and less on the spray edges where the spray angle was evaluated. Both types of images evidently show that the variations of these three fuels are similar.

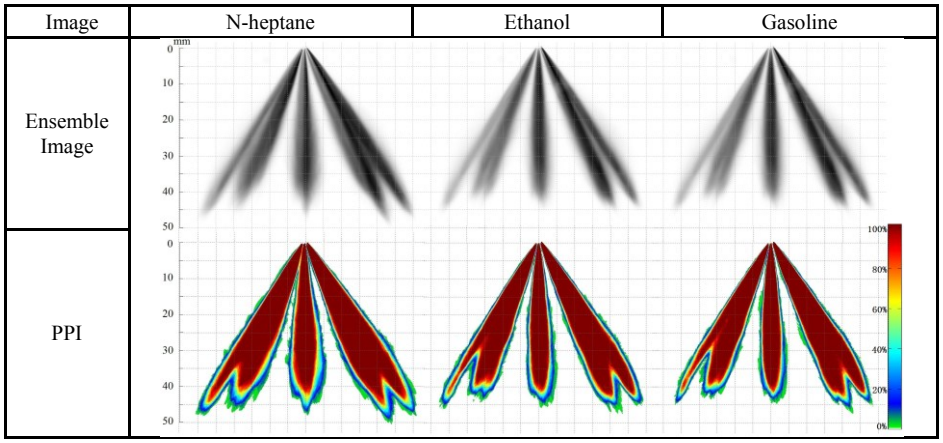

Figure 5 The Ensemble Images and PPIs of the three types of fuel.

Table 3 Spray Data Extracted from the ensemble image and PPI

Image	Character	Index	N-heptane	Ethanol	Gasoline
Ensemble Image	Penetration (mm)	Ave.	47.61	45.02	44.65
		SD	1.04	0.93	0.96
	Spray Angle (°)	Ave.	69.44	68.60	68.92
		SD	1.55	1.69	1.34
PPI	Penetration (mm)	5%	49.36	45.78	46.27
		95%	43.07	41.66	41.44
	Spray Angle (°)	5%	71.51	70.34	69.72
		95%	67.37	66.95	67.83

The spray data extracted from the ensemble images and PPI based on different fuels is shown in Table 3. Their spray cycle-to-cycle variation is illustrated in two bar graphs in Figs. 6 & 7. The COV of the three types of fuel is relatively small in the range of 1.93% to 2.27%. If illustrated in terms of the PVI, the spray tip PVI is about 12.75% for n-heptane and 9% for ethanol. The PVI of the spray angle are much lower than that of the spray tip penetration, in the ranges of 2.7% to 5.7%. Using PVI, it confirms that the liquid presence variation of spray angle was less than that of the penetration, in accordance with the pictures in Figure 5. Overall, the COV and PVI of spray penetration are similar with three types of fuel and the minimum ones are both for ethanol. It must be noted that the COV is an indication of variation relative to the mean value, while PVI implies the variation range based on the least probability.

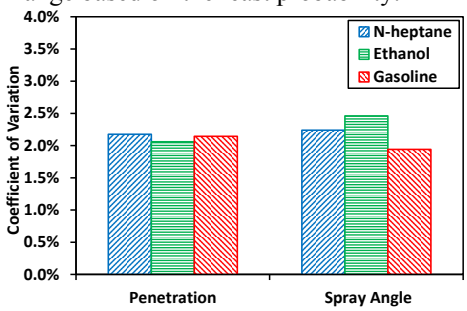

Figure 6 COVs of spray characters of three fuel types.

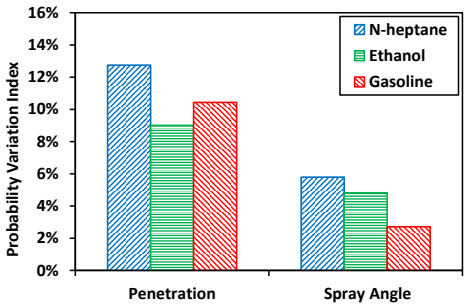

Figure 7 PVIs of spray characters of three fuel types.

2) Effects of Fuel Injection Pressure

Figure 8 depicts the ensemble images and PPIs of various injection pressures of n-heptane. At this condition, the n-heptane spray images were taken at the condition of 100 kPa back pressure with the fuel temperature and ambient temperature being 25 °C. Both images clearly show the spray angle and penetration increased with the rising of the injection pressure. By comparing the PPIs, the magnitudes of variation seem to be higher at elevated injection pressure.

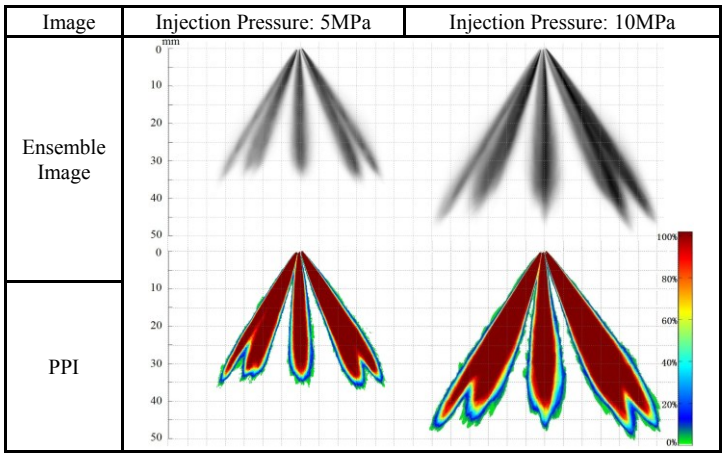

Figure 8 The Ensemble Images and PPIs of Different Injection Pressures of n-heptane.

The COV and PVI of spray angle and penetration along with different injection pressures for n-heptane are shown in Figs 9 & 10. With the increase of injection pressure, the COVs of spray penetration increase while that of spray angle is almost unchanged under different injection pressures. Similar to the COV trend, the PVIs of spray penetration increase with the spray angle staying almost the same with injection pressure rising, confirming what was found in the PPI images.

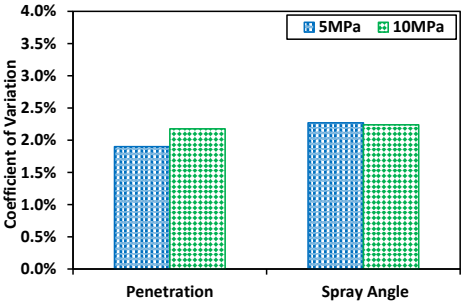

Figure 9 The COV of Spray Characteristics under Different Injection Pressures.

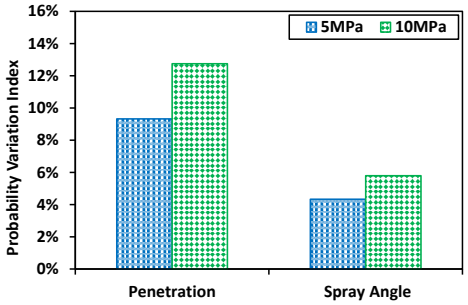

Figure 10 PVIs of Spray Characteristics under Different Injection Pressures.

3) Effects of Back Pressure

The effect of back pressure on spray variation is illustrated in Figure 11. The n-heptane spray images were taken under the conditions of 10 MPa injection pressure, the fuel temperature and ambient temperature being 25 °C with changing back pressures. With the increasing of back pressure, the spray penetration was restrained and became shorter while the variation slightly increased.

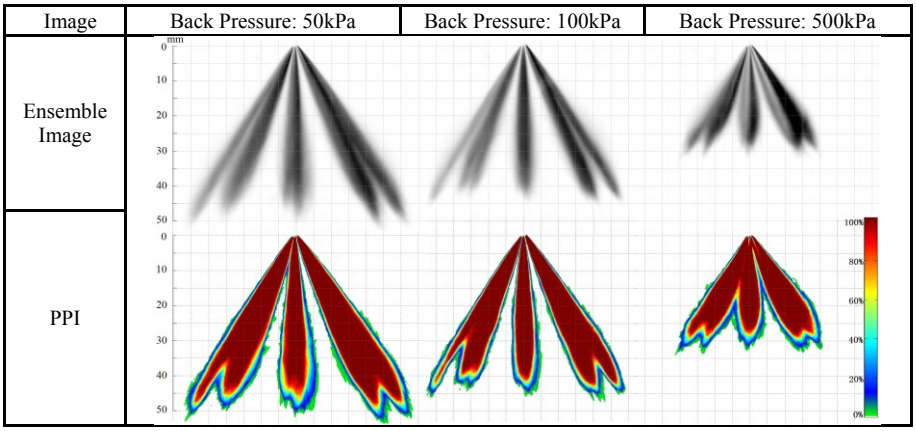

Figure 11 The Ensemble Images and PPIs of different injection pressures of n-heptane.

The data analyses of back pressure on the spray cycle-to-cycle variation are illustrated in Figs. 12 & 13. The COVs and PVIs of n-heptane spray penetration and spray angle along with the same fuel temperature of 25 °C and injection pressure of 10 MPa, but different back pressures are shown in bars. For n-heptane, the COVs and PVIs of spray characteristics are higher when the back pressure rises to 500kPa while they drop to the smaller values at the 100kPa back pressure condition. It is possible that a larger variation occurred at the higher back pressure.

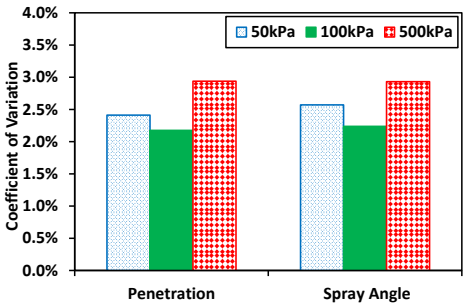

Figure 12 COVs of spray characters under different back pressures.

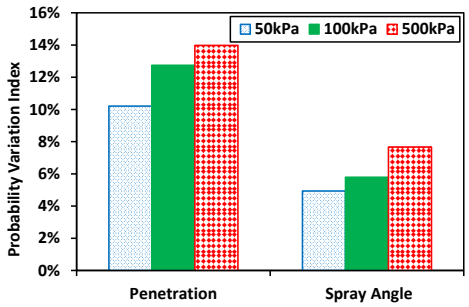

Figure 13 PVIs of spray characters under different back pressures.

4) Effects of Fuel Temperature

The ensemble images and PPIs of various fuel temperatures of n-heptane at the condition of 10 MPa injection pressure, 100 kPa back pressure with the ambient temperature being 25 °C are shown in Fig. 14. However, more variation still appeared at the highest temperature with elaborate observation. The data analysis of n-heptane spray penetration and spray angle along with different fuel temperatures for n-heptane are displayed in Figs. 15 & 16. With the increase of the temperature, both the COVs and PVIs of spray penetrations have similar trends that they first reduce to the minimum at 25 °C and then rise to higher values when it reaches 80 °C. The largest COV and PVI of spray angle for n-heptane both occur at 25 °C.

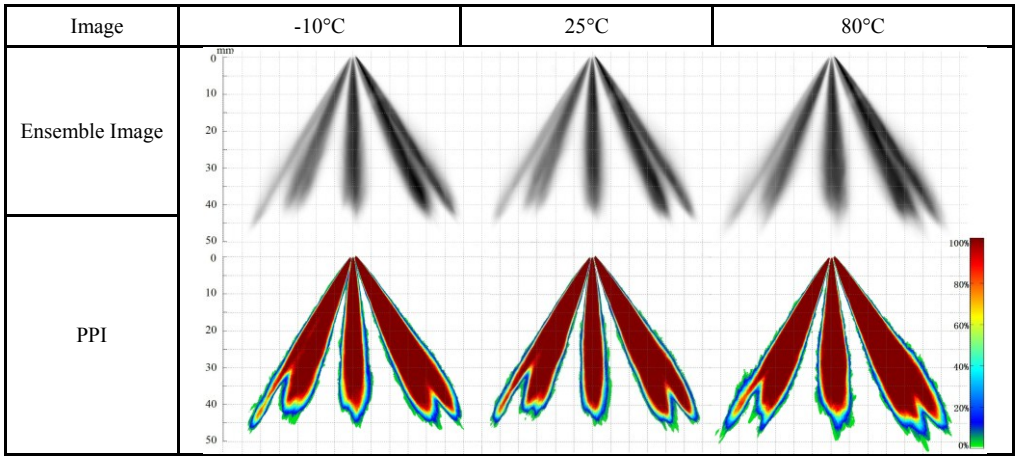

Figure 14 The Ensemble Images and PPIs of different injection pressures of n-heptane.

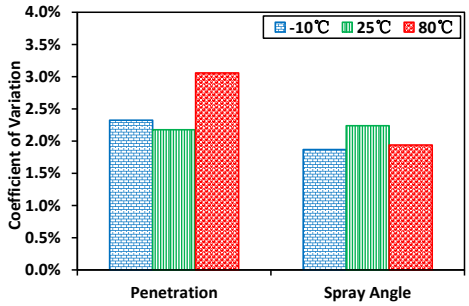

Figure 15 COVs of spray characteristics under different fuel temperatures.

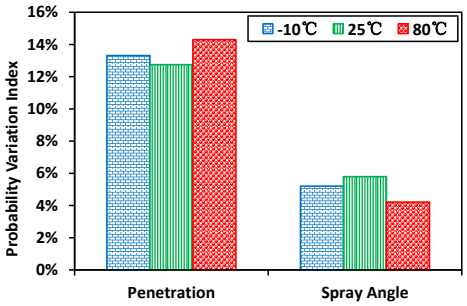

Figure 16 PVIs of spray characteristics under different fuel temperatures.

Summary Remarks

This paper investigated and quantified the cycle-to-cycle variations of pulsing spray characteristics of a multi-hole SIDI fuel injector under a wide range of test conditions. The image processing analysis containing both the ensemble image and PPI were used to show the variations of pulsing spray characteristics. The ensemble images generally have a good indication of the spray shape and the PPIs illustrate the variation distribution of the overall spray liquid presence. The PPI could be usefully represented in a quantitative manner based on monitoring the liquid presence variation over the injection cycles. Thus, this analysis approach is valuable for evaluating the magnitude and pattern of start of fuel cycle-to-cycle variation of fuel injectors. While an ensemble image provides qualitative information of variations, the PPI approach extends into a 2-D useful visualization method which can also extract the quantitative information of cycle-to-cycle spray variation. There is more variation along the spray tip than around the spray tip where the spray angle is measured. The data analysis using the COV and PVI parameters seem to work well when illustrating the variation extent. The trends can convey insightful information about the location and condition of the spray variation. Overall, the magnitudes of variations are very similar in both methods. A few remarks can be drawn from this study:

1) The spray structure of n-heptane seemed to possess larger variations than that of ethanol and gasoline. The physical properties of the n-heptane with the lower viscosity and surface tension could contribute to the enhanced evaporation of n-heptane spray.
2) At higher injection pressure, stronger vaporization occurred such that the variation was also increased.
3) When the fuel injected under high back pressure, the increased air density in the ambient could dominate the fuel formation process, so the larger variation occurred under the elevated back pressure. Likewise, the highest back pressure also showed the largest variation of the spray structure.
4) The higher temperature vaporized the fuel to a higher extent, and more variation appeared accordingly.

Future work is planned on studying the nature of cycle-to-cycle variations in the fuel mixture formation and combustion processes of fuel injected engines. In addition, at higher fuel temperature, flash boiling may occur if the actual vapor pressure is greater than the ambient pressure of the spray injection. Therefore, the current analysis techniques could also be used to study the cycle-to-cycle variation of flash boiling spray.

Acknowledgements

The research was carried out at National Engineering Laboratory for Automotive Electronic Control Technology in Shanghai Jiao Tong University.

References

[1] F. Zhao, M.C. Lai, and D.L. Harrington. Automotive spark-ignited direct-injection gasoline engines. *Progress in energy and combustion science*, 25(5):437–562, 1999.

[2] DP Towers and CE Towers. Cyclic variability measurements of in-cylinder engine flows using high-speed particle image velocimetry. *Measurement Science and Technology*, 15:1917, 2004.

[3] LI Davis Jr., LA Feldkamp, JW Hoard, F. Yuan, FT Connolly, CS Daw, and JB Green Jr. Controlling cyclic combustion variations in lean-fueled spark-ignition engines. 2001.

[4] M. Bysveen, T. Alms, K. Ulvund, and A. Jrgensen. Development of a shadowgraph image technique describing the fuel spray behavior in a rapid compression machine. *SAE Technical Paper*, No. 2004-01-2934, 2004.

[5] R. Schiessl, A. Dreizler, and U. Maas. Comparison of different ways for image postprocessing: detection of flame fronts. *SAE Technical Paper*, No. 1999-01-3651, 1999

[6] K. Kunkulagunta. Video imaging and analysis of common-rail sprays in an optical engine using shadowgraphy technique. *SAE Technical Paper*, No. 2000-01-1255, 2000.

[7] P.J. Tennison, T.L. Georjon, P.V. Farrell, and R.D. Reitz. An experimental and numerical study of sprays from a common rail injection system for use in an HSDI diesel engine. *SAE Technical Paper*, No. 980810, 1998.

[8] BD Stojkovic and V. Sick. Evolution and impingement of an automotive fuel spray investigated with simultaneous MIE/LIF techniques. *Applied Physics B: Lasers and Optics*, 73(1):75–83, 2001.

[9] M. Zaller, RJ Locke, and RC Anderson. Comparison of techniques for non-intrusive fuel drop size measurements in a subscale gas turbine combustor. *Journal of Visualization*, 2(3):301–308, 2000.

[10] L. Araneo, A. Coghe, G. Brunello, and GE Cossali. Experimental investigation of gas density effects on diesel spray penetration and entrainment. *SAE Technical Paper*, No. 1999-01-0525, 1999.

[11] J. Shao, Y. Yan, G. Greeves, and S. Smith. Quantitative characterization of diesel sprays using digital imaging techniques. *Measurement Science and Technology*, 14:1110, 2003.

[12] CT Chang and PV Farrell. A study on the effects of fuel viscosity and nozzle geometry on high injection pressure diesel spray characteristics. *SAE Technical Paper*, No. 970353, 558–567, 1997.

[13] J.M. Desantes, J. Arregle, J.V. Pastor, and A. Delage. Influence of the fuel characteristics on the injection process in a DI diesel engine. *SAE Technical Paper*, No. 980802, 1998.

[14] K. Yamane, A. Ueta, and Y. Shimamoto. Influence of physical and chemical properties of biodiesel fuels on injection, combustion and exhaust emission characteristics in a direct injection compression ignition engine. *International Journal of Engine Research*, 2(4):249, 2001.

[15] E. Alptekin and M. Canakci. Determination of the density and the viscosities of biodiesel-diesel fuel blends. *Renewable Energy*, 33(12):2623–2630, 2008.

[16] AM Murray and L.A. Melton. Fluorescence methods for determination of temperature in fuel sprays. *Applied optics*, 24(17):2783–2787, 1985.

[17] B.S. Higgins, C.J. Mueller, and D.L. Siebers. Measurements of fuel effects on liquid-phase penetration in DI sprays. *SAE Technical Paper*, No. 1999-01-0519 ,108(3):630–643, 1999.

[18] CN Grimaldi, L. Postrioti, C.C. Stan, and R. Trger. Analysis method for the spray characteristics of a GDI system with high pressure modulation. *SAE Technical Paper*, No. 2000-01-1043, 2000.

[19] E. Delacourt, B. Desmet, and B. Besson. Characterisation of very high pressure diesel sprays using digital imaging techniques. *Fuel*, 84(7-8):859–867, 2005.

[20] D.L.S. Hung, G.G. Zhu, J.R. Winkelman, T. Stuecken, H. Schock, and A. Fedewa. A high speed flow visualization study of fuel spray pattern effect on mixture formation in a low pressure direct injection gasoline engine. *SAE Technical Paper*, No. 2007-01-1411, pages 01–1411, 2007.

[21] D.L.S. Hung, D.M. Chmiel, and L.E. Markle. Application of an imaging-based diagnostic technique to quantify the fuel spray variations in a direct-injection, spark-ignition engine. *SAE Technical Paper*, No. 2003-01-0062, 2003.

[22] D.L.S. Hung and J. Zhong. Experimental analysis of the start of fuel cycle-to-cycle variations of solenoid-actuated high pressure fuel injectors. *SAE Technical Paper*, No. 2011-01-1882, 2011.

[23] D.L.S. Hung, D. Harrington, A. Gandhi, L. Markle, S.E. Parrish, J.S. Shakal, H. Sayar, S.D. Cummings, and J.L. Kramer. Gasoline fuel injector spray measurement and characterization-a new SAE J2715 recommended practice. *SAE Int. J. Fuels Lubr*, No. 2008-01-1068, 1(1):534–548, 2008.

[24] J.C. Russ. *The image processing handbook*. CRC, 2007.